International Journal of Nanoelectronics and Materials
Volume 13, No. 2, Apr 2020 [341-350]

Effect of Annealing on the Structural and Magnetic Properties of $SrFe_{12}O_{19}$-$CoFe_2O_4$ Nanocomposites

N. Idayanti[1,2], Dedi[2] and A. Manaf[1*]

[1]*Faculty of Mathematics and Natural Sciences, Department of Physics, Graduate Study in the Materials Science Program, Universitas Indonesia, Depok 16424, Indonesia.*
[2]*Research Center for Electronics and Telecommunications, Indonesian Institute of Sciences, Jl. Sangkuriang, Bandung 40135, Indonesia.*

Received 30 October 2019, Revised 5 February 2020, Accepted 17 March 2020

ABSTRACT

Single-phase $SrFe_{12}O_{19}$ (SHF) and $CoFe_2O_4$ (COF) crystalline powders obtained from the mechanical alloying process were mixed with aqueous media with mass proportions of 80:20 and then irradiated ultrasonically. Composite samples were made from dry powder mixing and then compacted through a compacting process in a cylindrical mould to produce green compact samples. The green composite samples were sintered at different temperatures of 1100°C, 1150°C, and 1200°C for two hours. Observation of the microstructure of the samples confirmed that all the samples had a composite structure consisting of SHF and COF particles. The mean size of the particles in the composite samples was much larger than the mean crystallite sizes of SHF and COF. The two types of particles in the composite were randomly distributed with no preferred orientation. The results of the evaluation of the magnetic properties of the composite samples showed that the magnetic properties were between those of SHF and COF. It was found that the optimal value was obtained when the sample was sintered at 1200°C, producing a remanence of M_r = 38.11 emu/g, saturation magnetization of M_s = 67.42 emu/g, and maximum energy product of $(BH)_{max}$ = 1.85 MGOe.

Keywords: Composite Magnets, Crystallites, $SrFe_{12}O_{19}$, $CoFe_2O_4$, Magnetic Properties.

1. INTRODUCTION

Nanocomposite magnets have drawn much attention due to their enhanced magnetic properties when hard and soft magnetic phases are in intimate contact [1]. The magnet, consisting of hard and soft magnetic phases in a composite structure, utilizes saturation magnetization of the soft phase with a value greater than that of the saturation magnetization of the hard-magnetic phase. The increase in the magnetic properties is caused by the occurrence of grain exchange interaction effects between the hard and soft phases [2]. The effect of this grain exchange interaction leads to a unified composite system as if a magnet with a new single phase with the saturation magnetization value lies between the saturation magnetization values of the two phases in the composite. The grain exchange effect also affects the magnetocrystalline anisotropic constant [3], which determines the coercivity of the nanocomposite magnet. The grain interaction effect increases the remanence, M_r. If the coercivity value is sufficient [4], increasing the value of M_r increases the value of the maximum energy product $(BH)_{max}$ as a function of $M_r^2/4\mu_0$.

M_r and $(BH)_{max}$ are the most common figures of merit for permanent magnets, which should be sufficiently high. Along with the development of today's technology, the components that are most expected as part of technology products are those that are made of materials with minimal

---

*Corresponding Author: *azwar@sci.ui.ac.id*

dimensions but can still meet the demands of product needs. In other words, in the case of permanent magnets, powerful permanent magnets require large M_r and $(BH)_{max}$ values. Rare earth permanent magnets such as NdFeB [5] and SmCo [6] have these properties; however, the expensive price of rare earth metals and low corrosion resistance of NdFeB magnets limit the use of these magnets. Additionally, the price and availability of SmCo magnets are the most relevant limitations to their use.

In contrast to rare earth permanent magnets, hard ferrites still dominate the market because of their low cost, excellent corrosion resistance, chemical stability against temperature changes and corrosive atmospheres, abundant raw materials and low-cost production. Nevertheless, hard ferrite magnets have low M_r and $(BH)_{max}$ values compared to those of rare earth magnets. For instance, barium hexaferrite, $BaFe_{12}O_{19}$ (BHF), has a saturation magnetization value of 0.38 T [7] and an anisotropy field of H_A = 16.4 kOe [8]. With such high intrinsic properties, the anisotropic BHF magnet can potentially lead to a theoretical 30.42 kJ/m^3 for $(BH)_{max}$ and 7.22 kJ/m^3 for isotropy. Hence, improving the magnetic properties of hexagonal ferrites while maintaining the low cost and reliability of these magnets is an interesting topic. One way to improve the magnetic properties of BHF may be through exchange spring effects between hard and soft magnetic phases in a nanocomposite magnet. The composite combines the high saturation magnetization of the soft phase with the high coercivity of the hard phase [9].

The magnetic exchange spring was formerly proposed by Kneller and Hawig [10], introducing a simulation model of the effect of exchange coupling between hard and soft magnetic phases in nanocomposite systems [11]. The saturation magnetization of magnetic spinels such as $CoFe_2O_4$ [12], Fe_3O_4 [13], $MnFe_2O_4$ [14] and $Ni_{1-x}Zn_xFe_2O_4$ [15] is higher than that of BHF, and these materials are good candidates for composite magnets. The coercivity (H_cJ) of BHF-$ZnFe_2O_4$ composite magnets was found increased. The M_r of BHF-$CoFe_2O_4$ was reported increased [12]. Many more experimental works and preparation methods have reported an increase in the magnetic properties of BHF-spinel composite magnets [16][17]. All the research works on BHF-spinel composites showed that the enhancements in the J_r and J_s of the composite magnets compared with those of the parent BHF phase can be achieved by the magnetic exchange spring effect. Microstructure observations showed that the two phases are well distributed and that the grain size of the composite is approximately 100-500 nm [18]. The hysteresis loop for such a magnet shows the effect of the exchange spring between the hard and soft magnetic phases. Nanocomposite magnets are characterized by remanence enhancement due to grain exchange interactions and increases in their saturation magnetization value. When a sufficiently high coercivity value is obtained for nanocomposite magnets, an improvement in the $(BH)_{max}$ value can be expected. This was shown in previous reports on the magnetic properties of $SrFe_{12}O_{19}/CoFe_2O_4$ nanocomposite magnets prepared through solid-state reactions [19], electrospinning [20], and the two-step coprecipitation method [21]. Through these methods, the hysteresis loops for the nanocomposites still show hard magnetization behaviour with remanence enhancement. The remanence enhancement was increased due to the exchange coupling interaction effect occurring strongly in $SrFe_{12}O_{19}/CoFe_2O_4$ nanocomposite magnets.

In this work, the structural and magnetic properties of the composite $SrFe_{12}O_{19}/CoFe_2O_4$ prepared through a mechanical alloying method and high-power ultrasonic irradiation with various sintering temperatures were observed. The structural and magnetic properties of the composite magnets were studied by X-ray diffraction (XRD) and a permagraph, respectively. This paper is aimed at adding information about the changes in magnetic properties arising from the exchange spring effect between the hard and soft magnetic phases of SHF and COF.

2. MATERIAL AND METHODS

2.1 Synthesis of $SrFe_{12}O_{19}$ and $CoFe_2O_4$

SHF was prepared by mechanically alloying stoichiometric amounts of Fe_2O_3 (E-Merck > 99%) and $SrCO_3$ (E-Merck > 99%). The precursors were mixed in a planetary ball milling machine with stainless steel balls. The mass ratio between the precursors and the balls was fixed at 1:10. Both the precursors and balls were then poured into a vial. Alcohol was added to the vial during the 8 hours wet milling process. The obtained powders were dried and subsequently calcined at 1200°C for 3 hours. The calcined powder was then re-milled together with SiO_2 and CaO additives for 8 hours. The fine calcined powders (3.5 grams) with 1.5% polyvinyl alcohol (PVA) added as a binder were compacted at a load of 5 tons by a hydraulic press machine. The green compact was then sintered at 1250°C for 1 hour. Some other powders were used to prepare the composite magnets.

A similar route was employed to prepare the COF. The stoichiometric amounts of precursors consisting of Fe_2O_3 and $CoCO_3$ powders were mixed in the planetary ball mill for 10 hours. The milled powders were then calcined at 1000°C for 2 hours. The fine COF powders (3.5 grams) with 1.5% PVA were compacted by a load of 5 tons, and then the compacted sample was sintered at 1000°C for 2 hours.

2.2 Synthesis of $SrFe_{12}O_{19}/CoFe_2O_4$ Composite Magnets

The composite of $SrFe_{12}O_{19}/CoFe_2O_4$ magnets with a composition by weight ratio of SHF: COF = 80/20 was prepared first through ultrasonic mixing of the crystalline powder materials under ultrasonic irradiation. Thirty grams of the powder mixture of SHF and COF was dissolved into 300 ml distilled water in a straight glass tube. An ultrasonic process was then performed at a frequency of 20 kHz for 10 hours. When the samples were well dispersed, a homogeneous suspension had formed. The particles were then separated from the water, collected and dried at 100°C for 3 hours. The second step was compacting the dried mixture particles under a cylindrical die. The green compact samples were sintered at temperatures of 1100°C, 1150°C, and 1200°C. Codes CMP1, CMP2 and CMP3 refer to the composite sample after sintering at temperatures of 1100°C, 1150°C, and 1200°C, respectively.

2.3 Characterization

The crystalline powders of SHF and COF were analysed by a Bruker D8 series X-ray diffractometer (XRD) using Cu Kα (λ = 1.5418 Å) radiation for 2θ ranging from 20° to 80°. The microstructure of each sample was observed under a JEOL-JSM IT-300 scanning electron microscope (SEM). The magnetic properties were evaluated by a permagraph (MAGNET-PHYSIK Dr. Steingroever GmbH).

3. RESULTS AND DISCUSSION

The diffraction patterns of the SHF, COF and composite samples are compared in Figure 1, along with the peak identification results. The first two patterns plotted in the bottom part of Figure 1 confirm that the SHF (JCPDS No. 33-1340) and COF (JCPDS No. 22-1086) samples are both single-phase materials. Obviously, the two patterns of the SHF and COF phases still exist in all the XRD patterns of composite samples without the emergence of any additional diffraction peaks.

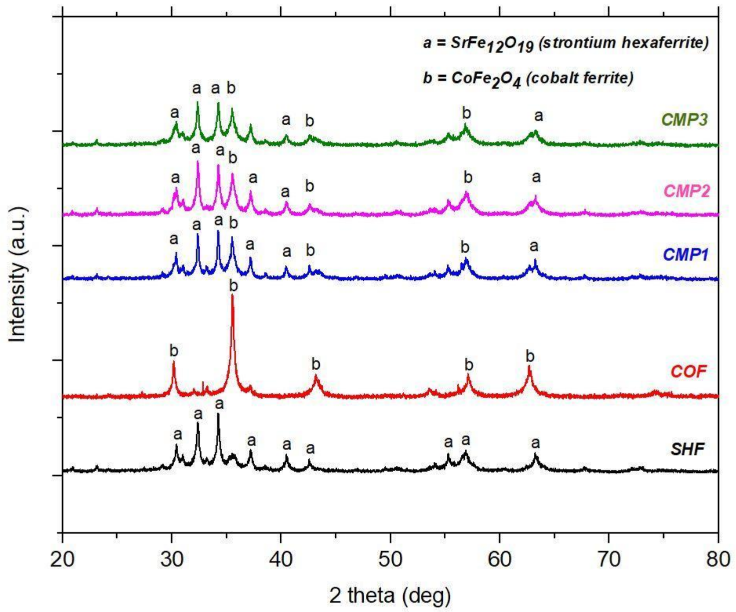

Figure 1. XRD patterns of SHF, COF and composite magnets.

The diffraction peaks appear to be present with relatively low intensity due to peak broadening caused by diffraction of fine crystals and microstrain effects. These two effects can be evaluated by equation (1), a Williamson Hall plot [22].

$$\beta_{\mathrm{hkl}}\, cos\, \theta \;=\; \frac{K\lambda}{D} + 4€\, sin\, sin\, \theta \qquad (1)$$

where β is the full width at half maximum (FWHM), θ is the Bragg angle, K is the Scherrer constant of 0.9, λ is the X-ray wavelength of 1.54 Å, D is crystallite size (nm), and € is the microstrain. The data are plotted with 4€ $sin\, sin\, \theta$ along the x-axis and $\beta_{hkl}\, cos\theta$ along the y-axis. The microstrain was determined from the slope of the right line, and the crystallite size value was determined from the interception of the fitting line and strain. Table 1 summarizes the lattice parameters of the individual phases, the microstrain, and the mean crystallite size of the SHF, COF, and composites. The mass fractions of the individual phases in the samples are also included in Table 1.

The results of the quantitative analysis of the sample composition in terms of the SHF and COF mass fractions, as listed in Table 1, show a change from the designated composition after sintering treatment with an increase in the SHF mass fraction accompanied by a decrease in the COF mass fraction. Changes in the initial composition of the composite SHF/COF (80/20) can indicate that diffusion between transition metals has occurred during sintering.

The lattice constants of the individual phases in all the composite samples mostly show values similar to three significant digits. This indicates that the individual phases of SHF and COF have no significant lattice distortion in the composite samples, which can also be seen from the insignificant microstrain values. No individual phase changes occur during sintering. The individual phases in the composite sample remain present as a physical mixture between the two phases. The mean crystallite sizes of COF and SHF are 30 nm and 29 nm, respectively. In the composite samples, the crystallite size of SHF undergoes insignificant crystallite growth due to sintering treatment. However, the crystallites of COF decrease compared with those of SHF. The two magnetic phases have crystallite sizes in the nanometre regime.

Table 1 Summary of quantitative analysis results of XRD data for SHF, COF, and composite magnets

Samples	Identified phase	Mass fraction (wt.%)	Lattice constant [Å]			Microstrain	Mean crystallite size[nm]
			a	b	c		
SHF	$SrFe_{12}O_{19}$	100	5.87914	5.87914	23.05940	0.0021	29
CMP1	$SrFe_{12}O_{19}$	89.3	5.88127	5.88127	23.04629	0.0090	45
	$CoFe_2O_4$	10.7	8.38107	8.38107	8.38107	0.0010	16
CMP2	$SrFe_{12}O_{19}$	91.8	5.88094	5.88094	23.06279	0.0022	40
	$CoFe_2O_4$	8.2	8.38045	8.38045	8.38045	0.0023	24
CMP3	$SrFe_{12}O_{19}$	92.6	5.88116	5.88116	23.06851	0.0021	31
	$CoFe_2O_4$	7.4	8.38531	8.38531	8.38531	0.0024	16
COF	$CoFe_2O_4$	100	8.38450	8.38450	8.38450	0.0026	30

Figure 2 shows micrographs of the fracture surfaces of SHF and COF. The crystallites of the SHF and COF were both agglomerated and present at different sizes of agglomerates. The mean particle size of SHF is larger than 1 µm, whereas that of COF is smaller than 1 µm.

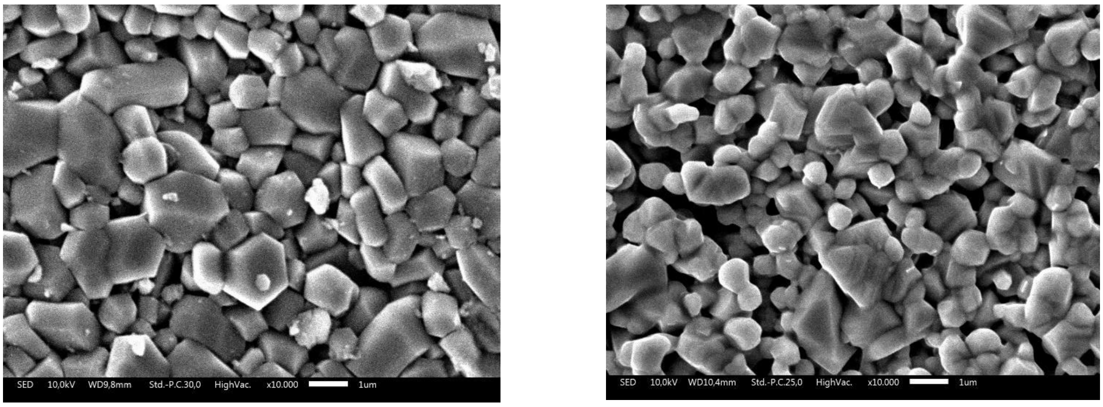

(a) (b)

Figure 2. SEM images of fracture surfaces of (a) SHF and (b) COF.

Figure 3 shows a series of micrographs of the fracture surfaces of composite magnets sintered at different temperatures from 1100°C to 1200°C. It is hard to see the crystallites, but the clusters of SHF and COF are visible. Visually, the connectivity among the clusters is improved with sintering treatment, where the higher the sintering temperature is, the larger the size of the clusters and the denser the microstructure with fewer pores. The clusters must have consisted of SHF or COF crystallites, as confirmed by the results of spot microanalysis at selected points, as shown in Figure 4. The size of the SHF is larger than that of the COF can also be seen visually in Figure 2 when each is present as a single-phase sample. According to the data in Table 1, the mean crystallite size of the SHF in the CMP samples ranges from 31 nm to 45 nm. According to the data in Table 1, the mean crystallite size of the SHF in the CMP samples ranges from 31 nm to 45 nm. The mean crystallite size of the COF in the CMP samples ranges from 16 nm to 24 nm. The magnetic crystallites within the clusters of SHF and COF in the CMP samples must undergo exchange interaction effects due to the fine crystallite sizes.

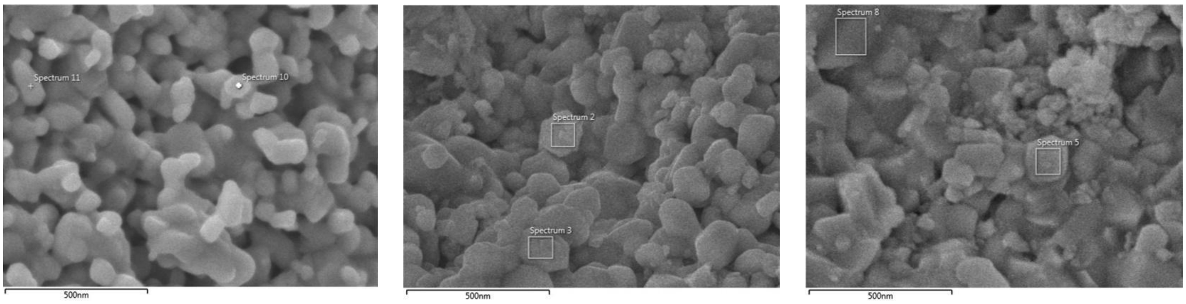

(a) (b) (c)

Figure 3. SEM images of fracture surfaces of (a) CMP1, (b) CMP2 and (c) CMP3 sintered at temperatures of 1100°C, 1150°C and 1200°C, respectively.

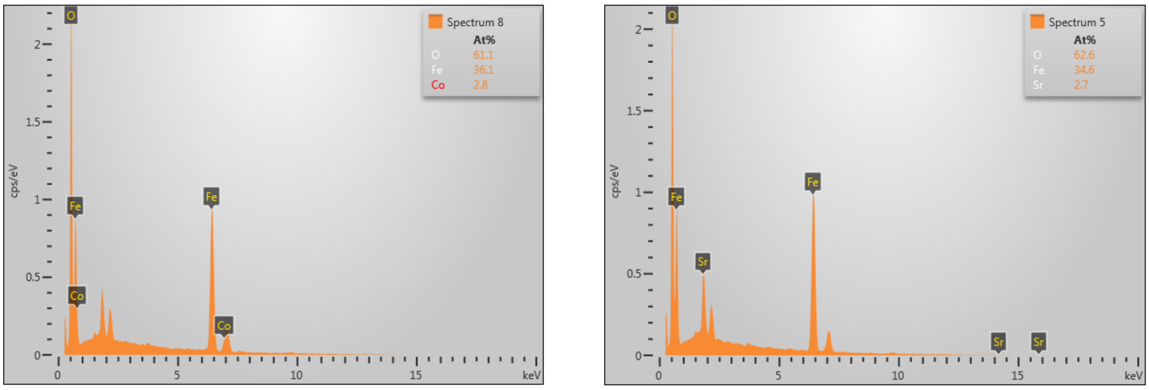

(a) (b)

Figure 4. Typical EDS spectra of microanalysis at a selected point, showing the presence of (a) SHF and (b) COF phases in the CMP samples.

The hysteresis loops of the composite samples (CMP), SHF and COF are compared in Figure 5, along with the inset plots of the second quadrant. The magnetic properties consisting of the remanence, coercivity, saturation magnetization and maximum energy product evaluated from the hysteresis loops are summarized in Table 2. The term "saturation magnetization, M_s" implies that the quoted value is the magnetization value at a magnetizing field of 12 kOe, which must be lower than the theoretical saturation magnetization. In Table 2, the remanence to saturation magnetization ratio values were obtained based on the value of M_r and the saturation magnetization M_s was obtained from the hysteresis loop. The hysteresis loop of SHF shows a loop typical of hexagonal ferrite. Referring to Table 2, the M_r/M_s for the SHF sample exceeds the theoretical limit of 0.5. The mean crystallite size of the SHF sample is 29 nm, which is much smaller than the exchange length of SHF of 40 nm [23]. Hence, the effect of the grain exchange interaction [24] must take place in the sample and explains the M_r/M_s value of >0.5. The hysteresis loop of COF shows a higher M_s value than that of SHF but with much lower coercivity. Moreover, the M_r/M_s ratio is slightly higher than 0.5. The mean crystallite size of the COF sample is 30 nm, which is comparable with that of SHF. The grain exchange effect must also be applied to the COF. The coercivity of the composite magnets is between the coercivity values of SHF and COF. The remanence of the composite magnets is similar to that of SHF. Although the grain exchange interaction effect takes place among crystallites of SHF and COF, the effect is believed to be less effective due to the relatively poor connectivity of the grain clusters (see Figure 3). Hence, the $(BH)_{max}$ of the CMP sample is lower than that of SHF, obviously due to a low H_c. Among the three CMP samples, CMP3 sintered at 1200°C possesses a high $(BH)_{max}$, which is obviously due to the better connectivity of grain clusters in this sample.

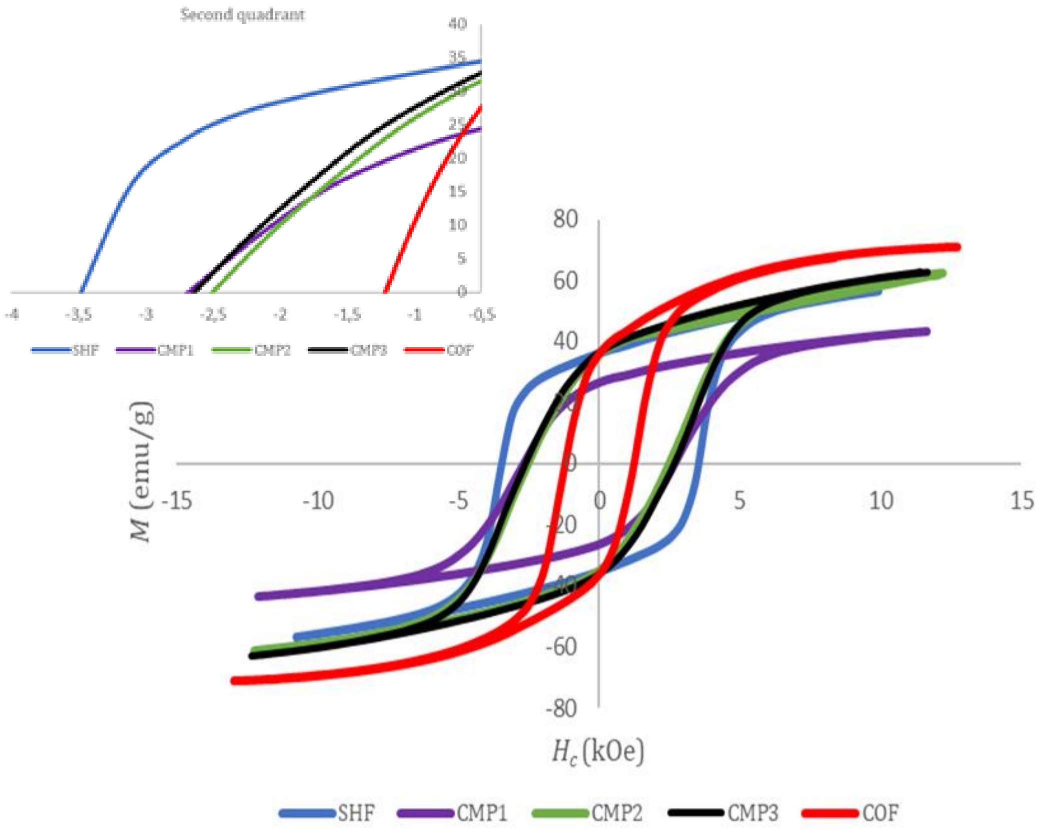

Figure 5. Full (M-H) loops and second quadrant for SHF, COF, and CMP magnets.

Table 2 Magnetic properties of SHF, COF and CMP

Samples	Remanence magnetization M_r (emu/g)	Magnetization saturation M_s (emu/g)	Remanence to saturation magnetization ratio $R = M_r/M_s$	Coercivity H_c (kOe)	Maximum energy product $(BH)_{max}$ (MGOe)
SHF	36.84	61.25	0.60	3.52	3.68
CMP1	27.06	46.88	0.58	2.60	1.54
CMP2	36.38	65.44	0.56	2.60	1.55
CMP3	38.11	67.42	0.56	2.82	1.85
COF	38.65	73.6	0.53	1.39	0.66

The M_s and H_c of the CMP samples against sintering temperature are plotted in Figure 6. The M_s and H_c values tend to increase with increasing sintering temperature. M_s and H_c reach maximum values of 67.42 emu/g for M_s and 2.82 kOe for H_c that correspond to sample CMP3. The increases in M_s and H_c ensure that interconnection between the grains determines the value of $(BH)_{max}$. The high M_S value determines the M_r, and the high H_c value determines the squareness of the second quadrant. The coercivity of nanocomposites sensitively depends on the phase composition and morphology such as the size and grain shape [25].

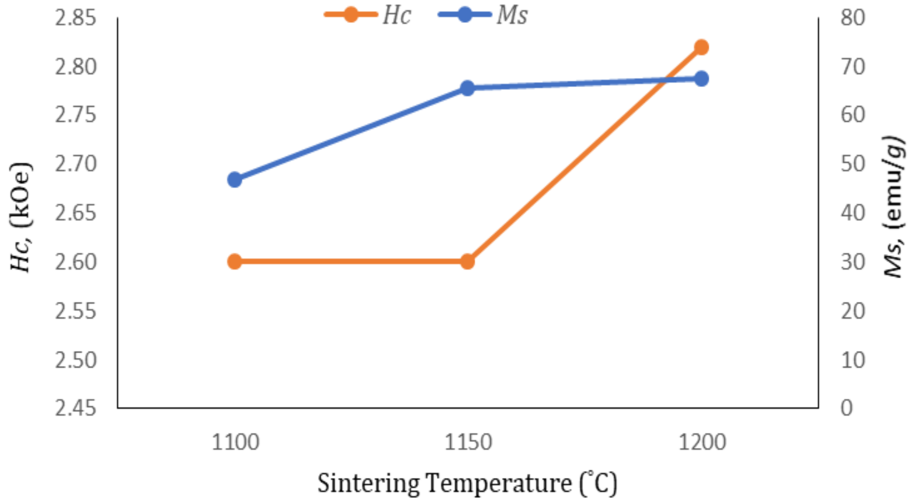

Figure 6. The tendencies of M_s and H_c of the composite versus sintering temperature of composites $SrFe_{12}O_{19}/CoFe_2O_4$.

Table 3 compares the M_S, H_c and $(BH)_{max}$ values of the SHF-COF composite magnets prepared through mechanical alloying followed by ultrasonic irradiation (MA-US) treatment, which has been applied to the current research work and other preparation methods by several researchers. The M_s value of 67.42 emu/g is only slightly below the M_s value of the hydrothermal process [29] but is superior to those of other methods [1, 18, 19, 20, 28]. Likewise, the coercivity value of 2.82 kOe is only lower than the value obtained from the coprecipitation method [20]. However, compared to other methods [1, 18, 19, 28, 29], the coercivity value of the current work is far superior. However, the $(BH)_{max}$ value obtained from the MA-US method is only superior to the solid-state reaction and electrospinning methods. Hence, a high remanent value is not directly determined by $(BH)_{max}$, which is calculated from $M_r^2/4\int_0$ [4].

Table 3 A comparison of the properties of the prepared SHF-COF composites by different methods

Method	**Saturation magnetization M_s (emu/g)**	**Remanent magnetization M_r (emu/g)**	**Coercive field H_c (kOe)**	***$(BH)_{max}$ (MGOe)***	**Ref.**
MA-US	67.42	38.11	2.82	1.85	This work
Coprecipitation	27.90	15.00	3.57	3.35 *(estimated)*	[21]
Coprecipitation high temp	42.50	25.1	2.48	3.69 *(estimated)*	[26]
Reduction process	60.90	30.45	1.25	2.38 *(estimated)*	[1]
Solid-state reaction	58.90	22.38	1.33	1.87 *(estimated)*	[19]
Electrospinning	62.80	31.21	2.29	1.29	[20]
Hydrothermal process	73.70	34.00	2.13	4.54 *(estimated)*	[27]

4. CONCLUSION

SHF-COF composites with a mass ratio of 80:20 were prepared by ultrasonic mixing between crystalline powders of SHF and COF. The effect of annealing treatment on the composite samples at a temperature of 1200°C resulted in better connectivity of grain clusters. The mean crystallite size of the COF in the CMP samples ranged from 16 nm to 24 nm. The mean crystallite size of the SHF in the CMP ranges from 31 nm to 45 nm, which was slightly larger than that of a single-phase SHF magnet (29 nm). The mean crystallite size of the COF in the CMP samples ranged from 16 nm to 24 nm. Although the annealing effect on composite magnets produced an M_r/M_s ratio value greater than 0.5, the $(BH)_{max}$ value obtained was still low due to insufficiently good connectivity of the grain clusters.

ACKNOWLEDGMENTS

We are thankful for the financial support provided by the Directorate of Research and Community Service Universitas Indonesia under the research project TADOK contract, no. NKB-0146/UN2.R3.1/HKP.05.00/2019, and for the technical support from the Research Centre for Electronics and Telecommunication-LIPI and the Research Unit for Clean Technology-LIPI. The authors also gratefully acknowledge the support of the Postgraduate Program of Materials Science at Universitas Indonesia.

REFERENCES

[1] Dong J., Zhang Y., Zhang X., Liu Q., and Wang J. Mater. Lett. **120** (2014) 9–12.
[2] Park J., *et al.* Sci. Rep. **7**, 2 (2017) 1–5.
[3] Herzer, G. J. Mat. Eng. Per. **2** (1993) 193-198.
[4] Skomski, R. J. Phys.: Condens. Matter **15** (2003) R841–R896.
[5] Kim A. S., Camp F.E. J. Appl. Phys. **79,** 8 (1996) 5035.
[6] Sayama J., Asahi T., Mizutani K., & Osaka T. J. Phys. D. Appl. Phys. **37**, 1 (2004).
[7] Sözeri H. J. Magn. Magn. Mater. **321,** 18 (2009) 2717–2722.
[8] Wang S. G., Yoon S. D., & Vittoria C. J. Appl. Phys. **92**, 11 (2002) 6728–6732.
[9] Rahman A., Jayaganthan R. Surf. Eng. **33**, 11 (2017) 810–815.
[10] Kneller E. F., Hawig R. IEEE Trans. Magn. **27**, 4 (1991) 3588–3600.
[11] Idayanti N., Manaf A. Metalurgi **1**, 1(2018) 1–18.
[12] Yang H. Mater. Chem. Phys. **160**, (2015) 5–11.
[13] Remya K. P., Prabhu D., Amirthapandian S., Viswanathan C., & Ponpandian N. J. Magn. Magn. Mater. **406** (2016) 233–238.
[14] Zhidong H. A. N., Limin D., Dawei Z., Ze W. U., & Xianyou Z Rare Metal **2**, 6 (2006) 462–465.
[15] Wang Y., Huang Y., & Wang Q. J. Magn. Magn. Mater. **324**, 19 (2012) 3024–3028.
[16] Nikmanesh H., Moradi M., Kameli P., Bordbar G. H. J. Electron. Mater. **46**, 10 (2017) 5933–5941.
[17] Yang H., Liu M., Lin Y., Yang Y. J. Alloys Compd. **631** (2015) 335–339.
[18] Durmus Z., Unal B., Toprak M. S., Sozeri H., Baykal A., Polyhedron **30**, 7 (2011) 1349–1359.
[19] Hilczer A., Kowalska K., Markiewicz E., Pietraszko A., Andrzejewski B. Mater. Sci. Eng. B Solid-State Mater. Adv. Technol. **207** (2016) 47–55.
[20] Pan L., Cao D., Jing P., Wang J., Liu Q. Nanoscale Res. Lett. **10**, 1 (2015) 1–7.
[21] Zhang L. Li Z., J. Alloys Compd. **469**, 1–2 (2009) 422–426.
[22] D. Chen *et al.,* “Morphology control of hexagonal strontium ferrite micro / nano-crystals Morphology control of hexagonal strontium ferrite micro/nano-crystals,” AIP Adv. 056214 (2017) 1–6.
[23] Song F., Shen X., Liu M., & Xiang J. J. Nanosci. Nanotechnol. **11**, 8 (2011) 6979–6985.
[24] Xu Y. F., Ma Y. Q., Xu S. T., Zan F. L., Zheng G. H., Dai Z. X. Mater. Res. Bull. **57** (2014) 13–18.

[25] Han G.B. *et al.* Appl. Phys. A Mater. Sci. Pro. **81**, 3 (2005) 579–582.
[26] Xie T., Xu L., Liu C. Powder Technol. **232** (2012) 87–92.
[27] Xia A. *et al.* J. Alloys Compd. **653**, (2015) 108–116.

[25] Han G.B. *et al.* Appl. Phys. A Mater. Sci. Pro. **81**, 3 (2005) 579–582.
[26] Xie T., Xu L., Liu C. Powder Technol. **232** (2012) 87–92.